Fuzzy Statistical Normalization CFAR Detector for Non-Rayleigh Data

YANWEI XU
CHAOHUAN HOU, Fellow, IEEE
SHEFENG YAN, Senior Member, IEEE
JUN LI
CHENGPENG HAO
Institute of Acoustics, Chinese Academy of Science
Beijing, China

A new constant false-alarm rate (CFAR) detector for non-Rayleigh data, based on fuzzy statistical normalization, is proposed. The proposed detector carries out the detection with two stages. The first stage of the fuzzy statistical normalization CFAR processor is background level estimation, based on fuzzy statistical normalization. The second stage is signal detection, based on the original data and the defuzzification normalized data. Performance comparisons are carried out to validate the superiority of the proposed CFAR detector.

Manuscript received October 23, 2013; revised March 18, 2014, June 4, 2014; released for publication June 11, 2014.

DOI. No. 10.1109/TAES.2014.130683.

This work was supported, in part, by the National Natural Science Foundation of China under Grants No. 61222107 and No. 61431020.

Refereeing of this contribution was handled by S. Watts.

Authors' addresses: Y. Xu, C. Hou, S. Yan, J. Li, C. Hao, Institute of Acoustics, Chinese Academy of Science, 21 North 4th Ring West Road, Haidian District, Beijing, 100190, China, E-mail: (sfyan@ieee.org).

I. INTRODUCTION

Constant false-alarm rate (CFAR) detection plays an important role in radar or sonar signal processing. Its basic principle is to set a decision about the presence or the absence of a target using the adaptive threshold techniques. A CFAR detector sets the threshold adaptively to maintain a CFAR according to the background information by processing the reference cells surrounding the cell under test (CUT) in range. According to the background distribution function, CFAR detectors can be divided into two classes: one is Rayleigh CFAR detectors, and the other is non-Rayleigh CFAR detectors.

Rayleigh CFAR detectors presume that the background is homogeneous and Rayleigh distributed. The typical and basic Rayleigh CFAR detector is the cell-averaging CFAR (CA-CFAR) detector [1]. The detection performance of the CA-CFAR is optimal when the background is homogeneous and the number of reference cells is large, while it decreases deeply in nonhomogeneous background. Many alternative CFAR processors have been proposed to adapt themselves to the nonhomogeneous environments, such as the smaller of CFAR (SO-CFAR) [2], the greater of CFAR (GO-CFAR) [3], and the order statistic CFAR (OS-CFAR) [4]. The SO-CFAR has a good capability of closely spaced targets interference suppression but has a worse detection capability than the CA-CFAR, if interfering targets are located in both the leading and lagging windows, and has excessive false alarms in the presence of clutter edges. The GO-CFAR has a good capability of boundary reverberation suppression, while it decreases greatly in multitarget conditions. The OS-CFAR detector has an advantage over the CA-CFAR, GO-CFAR and SO-CFAR detectors against multitargets, although it requires large processing time and suffers from excessive false alarms during clutter transitions [5, 6].

Non-Rayleigh CFAR detectors presume that the background is non-Rayleigh distributed. Non-Rayleigh distributions include Rayleigh mixture distribution, K distribution, Weibull distribution, etc. In recent years, many researchers have studied the properties of non-Rayleigh distributions in great detail, such as Rayleigh mixture distribution [7], K distribution [8–14], Weibull distribution[15–20], log-normal distribution [20], McDaniel model [21], clutter mixture model [22], generalized Pareto distribution [23], and spherically invariant random vector model [24]. However, most of the non-Rayleigh probability density functions (pdfs) have two parameters.

In recent years, fuzzy CFAR detectors have been widely studied, mainly for the use of multiple sensors [25–28]. The fuzzy CFAR detectors of distributed sensors replace the fixed threshold with a soft continuous threshold gained from the membership function. That is, the local sensors produce a soft decision (between 0 and 1), instead of a binary decision, and the fusion center executes CFAR data fusion through fuzzy integration. In [29], a fuzzy CFAR detector using a fuzzy logic controller

with three input variables for radar moving target detection systems was proposed.

In this paper, we propose a new robust CFAR detector based on fuzzy statistical normalization, called the fuzzy statistical normalization CFAR (FSN-CFAR) detector, for non-Rayleigh radar or sonar data in nonhomogeneous environment. The remainder of this paper is organized as follows: In Section II, the FSN-CFAR detection is introduced. We discuss some simulation results and a conclusion in Section III and conclude this paper in Section IV.

II. FSN-CFAR DETECTION

The detection performance of a CFAR detector is determined by the rational detection threshold. Irrational detection thresholds may result in the increase in the probability of false alarm (pf). For active sonar systems, the false alarms have traditionally been assumed to arise mainly from Rayleigh distribution reverberation. However, for the current high-resolution active sonar systems brought on by the high bandwidth and the large array size, the sources of echo may come from targets of interest, interfering objects having similar character to the target, bottom, sea surface, and other scatterers. The number of independent scatterers is not large enough relative to the size of the sonar system's resolution cell. This typically results in the high-resolution sonar data distribution diverging from the Rayleigh distribution to non-Rayleigh distribution, such as K distribution. In this section, the Rayleigh and K distributions are introduced first, then a fuzzy Rayleigh set and the normalization based on the fuzzy Rayleigh set are proposed, and finally, a fuzzy statistical normalization processor is presented.

A. Rayleigh Distribution Model

The pdf of Rayleigh distribution is

$$p(x) = \frac{x}{\sigma^2}\exp\left(-\frac{x^2}{2\sigma^2}\right) \quad x \geq 0. \tag{1}$$

Here, σ^2 is known as the fading envelope of the Rayleigh distribution.

The cumulative distribution function (cdf) of Rayleigh distribution is

$$P_R(x) = 1 - \exp\left(-\frac{x^2}{2\sigma^2}\right). \tag{2}$$

The mathematic expectation of Rayleigh distribution is

$$E[X] = \sqrt{\frac{\pi}{2}}\sigma. \tag{3}$$

From the pdf of Rayleigh distribution and its characteristics, we can see that the pdf has only one parameter, and the parameter σ can be estimated by the mathematic expectation. If the reverberation is Rayleigh distributed, and the detection threshold is S, the pf, P_f, is

$$P_f = \int_S^\infty p(x)dx = \exp\left[\frac{-S^2}{2\sigma^2}\right]. \tag{4}$$

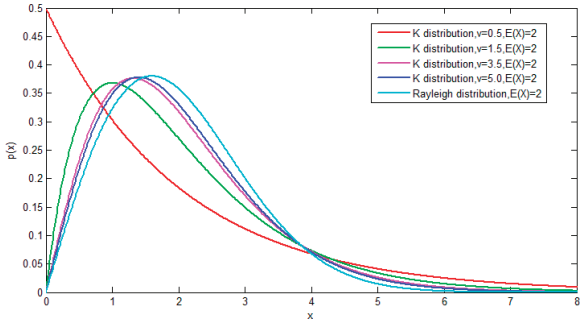

Fig. 1. Pdf comparison of Rayleigh and K distributions.

Equation (4) shows the relationship between the threshold value S and the P_f. That is, if S is fixed, the parameter σ will vary according to the changes of the information of variable x, and P_f will change accordingly. If we estimate the parameter σ with the mean of the variable x and make S vary according to the variation of the parameter σ, then P_f will not change with the variation of the parameter σ. This is the Rayleigh CFAR detection.

B. K Distribution Model

The pdf of K distribution is

$$p(x) = \frac{2}{a\Gamma(v)}\left(\frac{x}{2a}\right)^v K_{v-1}\left(\frac{x}{a}\right) \quad x \geq 0, v > 0, a > 0, \tag{5}$$

$$E\left[X^k\right] = (2a)^k \frac{\Gamma\left(\frac{k}{2}+1\right)\Gamma\left(v+\frac{k}{2}\right)}{\Gamma(v)} \quad k \geq 0, \tag{6}$$

where $\Gamma(\bullet)$ is the gamma function, $K_{v-1}(\bullet)$ is the $v-1$ order-modified Bessel function of the second kind, v is the shape parameter that determines the shape of K distribution, a is the scale parameter that is related to the average power of the K-distribution background.

C. Fuzzy Rayleigh Set

Fig. 1 displays the sample plots of the Rayleigh distribution pdf and the K-distribution pdf with different values of v. From Fig. 1, we can see that the K-distribution pdfs have longer tails and steeper heads than that of the Rayleigh distribution. The smaller value of v, the longer tail of the K-distribution pdf, and the K distribution tends toward a Rayleigh distribution as $v \to \infty$.

What makes the high-resolution sonar data distribution diverge from Rayleigh to K? The answer is the target echoes, the clutters, the lower shadow area noise, and so on. In active sonar, reverberation arises from the multiple reflections, diffusions, or diffractions of the transmitted signal by the sea surface, bottom, and elementary volume elements, such as fish, bubbles, and other inhomogeneities. However, the clutter here is caused by interfering targets, such as isolated rock outcrops, wrecks, and coral reefs, and is defined as the extended upper tail of the output

distribution in the absence of a target signal [30]. The lower shadow area noise refers to the lower power noise and lower power reverberation in the region screened by an object [31]. When the data values are available, there is uncertainty about the exact category of the data. This uncertainty is fuzziness, and the fuzziness of the data reflects the lack of exact knowledge of the echo sources.

From Fig. 1, we can see that the clutters or the target echoes, which are the extended upper tails of the K distribution, influence the shape parameter of K distribution and may not be the outliers of the K-distribution background data. In fact, the clutters or the target echoes are usually the outliers of the background data, and the normalization is needed to remove them in sonar or radar target detection. Because the Rayleigh distribution model has the only parameter σ, which is related to the average power of the background data, we design a fuzzy Rayleigh background set for the normalization of background data, and it is defined as $A = \{(x, \mu_A(x))|x \in X\}$. Here, A is the fuzzy set of Rayleigh reverberation, X is the universal set of the fuzzy data, x is the membership of the set X, and $\mu_A(x)$ is the membership function of the fuzzy set A. For each $x \in X$, the value of $\mu_A(x)$ is in [0, 1], and it reflects the degree of the fuzzy variable x belonging to the set A.

Based on (2), we can see that the cdf of Rayleigh distribution $P_R(x)$ is a monotonic increasing function and takes values from the interval [0, 1]. If x is the lower shadow area noise, its value will be very small, and $P_R(x)$ will be also very small. Conversely, if x is the clutter or a target echo, its value will be very large, and $P_R(x)$ will be also very large. From Fig. 1, we can see that no matter if the value of variable x is very small or large, its probability density is very small, and the degree of x belonging to the Rayleigh reverberation set A is small. Thus, we can follow that whether $P_R(x)$ is very small or very large, the value of $\mu_A(x)$ is very small, which means the degree of x belonging to the set A is very small.

For a constant amplitude signal x in Rayleigh interference, the task at hand is to select one of three hypotheses:

H_0: $x \le th_0$, shadow area noise,
H_1: $th_0 < x < th_1$, Rayleigh reverberation, or
H_2: $x \ge th_1$, clutter or target signal.

Here, th_0 is the crisp decision threshold to distinguish shadow area noise from Rayleigh reverberation. In addition, th_1 is the crisp decision threshold to distinguish Rayleigh reverberation from clutters or target echoes. Fig. 2 shows the relationships of th_0, th_1, and the parameter σ of the Rayleigh pdf.

If x_i is a single observation of Rayleigh distribution data, the probability that x_i is less than th_0 is

$$\Pr(x_i \le th_0) = \int_0^{th_0} p(x)dx = P_R(th_0). \tag{7}$$

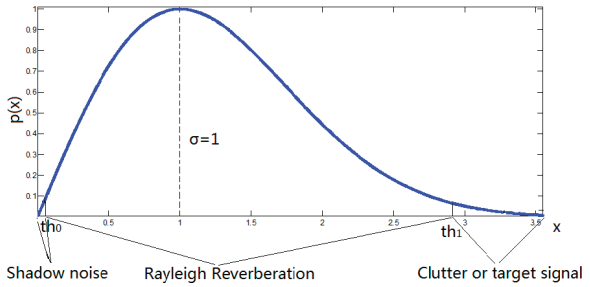

Fig. 2. Relationships of th_0, th_1 and parameter σ of Rayleigh pdf, here $\sigma = 1$.

The probability that x_i exceeds th_1 is

$$\Pr(x_i \ge th_1) = \int_{th_1}^{\infty} p(x)dx = 1 - P_R(th_1). \tag{8}$$

Equation (7) is monotonic increasing in the range[0, 1], while (8) is monotonic decreasing in the range [0, 1]. For the smaller x, which may come from the lower shadow area noise, the smaller the value of x and the smaller degree of x belonging to the set of Rayleigh reverberation are. Based on (7), the membership function $\mu_{As}(x)$, which maps the lower shadow area noise space to the Rayleigh reverberation space, is defined as

$$\mu_{As}(x) = P_R(x). \tag{9}$$

Similarly, for the greater x, which may be from the clutter or target echo, the greater the value of x and the smaller degree of x belonging to the set of Rayleigh reverberation are. Based on (8), the membership function $\mu_{Ag}(x)$, which maps the clutter or target echo space to the Rayleigh reverberation space, is defined as

$$\mu_{Ag}(x) = 1 - P_R(x). \tag{10}$$

For any kind of x, no matter if it comes from the lower shadow area noise, the clutter or target echo, or the reverberation, the membership function should be the intersection of $\mu_{As}(x)$ and $\mu_{Ag}(x)$. Based on (7) and (8), the membership function $\mu_A(x)$, which maps all the sonar envelope data space to the Rayleigh reverberation space, is defined as (11):

$$\begin{aligned}\mu_A(x) &= \mu_{As\cap Ag}(x) = \min(\mu_{As}(x), \mu_{Ag}(x)) \\ &= \begin{cases} P_R(x), & if\ P_R(x) \le 0.5, \\ 1 - P_R(x), & if\ P_R(x) > 0.5. \end{cases}\end{aligned} \tag{11}$$

To let $\max(\mu_A(x)) = 1$, the ultimate expression of $\mu_A(x)$ is (12):

$$\mu_A(x, \sigma) = \begin{cases} 2P_R(x) = 2\left(1 - \exp\left(-\dfrac{x^2}{2\sigma^2}\right)\right), & if\ P_R(x) \le 0.5, \\ 2(1 - P_R(x)) = 2\exp\left(-\dfrac{x^2}{2\sigma^2}\right), & if\ P_R(x) > 0.5. \end{cases} \tag{12}$$

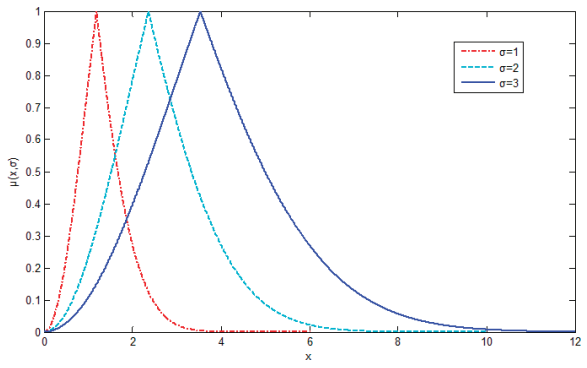

Fig. 3. Membership functions of fuzzy Rayleigh reverberation.

The corresponding membership functions $\mu_A(x, \sigma)$ are depicted in Fig. 3, with $\sigma = 1, 2, 3$, respectively.

D. Normalization Based on Fuzzy Statistical Inference and Defuzzification Operation

The normalization is needed to remove the nonstationarity of the active sonar reverberation [24]. In this paper, we propose a new normalization algorithm based on fuzzy statistical inference and defuzzification operation for non-Rayleigh distribution active sonar or radar data. This method realizes the outlier rejection by attenuating the heavier-tailed data and enlarging the lower shadow area noise data, based on the fuzzy Rayleigh set proposed in the last subsection (Section II.C).

From Fig. 3, we can see that if the minimum membership value of a fuzzy Rayleigh set is $x_{\min}$, $\mu_A(x_{\min}, \sigma) \to 0$, theoretically. Any variable whose value is smaller than $x_{\min}$ will be an outlier. Based on (12) and (2), if $\mu_A(x_{\min}, \sigma) = 0$, then $\exp(-\frac{x_{\min}^2}{2\sigma^2}) = 1$ and $\frac{x_{\min}^2}{2\sigma^2} = 0$. We are unable to obtain any information from $x_{\min}$ and parameter σ. Thus, we let $\mu_A(x_{\min}, \sigma) = 0.2$, if $x < x_{\min}$, then $P_R(x) < P_R(x_{\min}) = 0.1$, and x will be an outlier. If $x \geq x_{\min}$, then $\mu_A(x, \sigma) \geq \mu_A(x_{\min}, \sigma) = 0.2$, and x will be a membership of the Rayleigh reverberation set.

Similarly, if the maximum membership value of the fuzzy Rayleigh set is $x_{\max}$, $\mu_A(x_{\max}, \sigma) \to 0$, theoretically. Any variable whose value is greater than $x_{\max}$ will be an outlier. Also, based on (12) and (2), if $\mu_A(x_{\max}, \sigma) \to 0$, then $\exp(-\frac{x_{\max}^2}{2\sigma^2}) = 0$ and $\frac{x_{\max}^2}{2\sigma^2} = \infty$. We also are unable to obtain any information from $x_{\max}$ and parameter σ. Therefore, we also let $\mu_A(x_{\max}, \sigma) = 0.2$, if $x > x_{\max}$, then $P_R(x) > P_R(x_{\max}) = 0.9$, and x will be an outlier. If $x \leq x_{\max}$, then $\mu_A(x, \sigma) \leq \mu_A(x_{\max}, \sigma) = 0.2$, and x will be a membership of the Rayleigh reverberation set.

Here, defuzzification transforms the fuzzy active sonar data into the crisp Rayleigh reverberation data using the alpha-cut (α − cut) method. An $\alpha-$cut of a fuzzy set A is the crisp set A_α that contains all the elements that have the membership value greater than or equal to α, which is

$$A_\alpha = \{x \in X | \mu_A(x, \sigma) \geq \alpha\}. \tag{13}$$

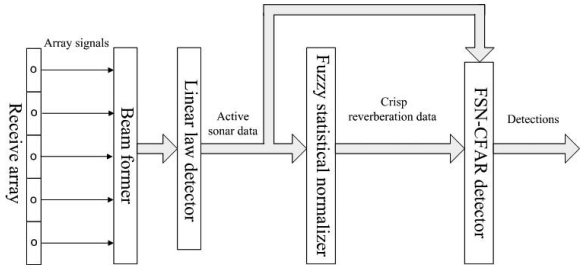

Fig. 4. Flow diagram of active sonar signal processing based on fuzzy statistical normalization.

We let $\alpha = 0.2$, and the $0.2 -$ cut set is

$$A_{0.2} = \{x \in X | \mu_A(x, \sigma) \geq 0.2\}. \tag{14}$$

Then, from (12) and (14), we can see that the variable x of the crisp Rayleigh reverberation set satisfies (11):

$$0.1 \leq P(x) \leq 0.9. \tag{15}$$

The crisp Rayleigh reverberation set is denoted as follows:

$$A_{0.2} = \{x \in X | 0.1 \leq P(x) \leq 0.9\}. \tag{16}$$

E. FSN-CFAR Detection

To introduce the FSN-CFAR detector clearly, the flow diagram of active sonar data processing for the FSN-CFAR detector is shown in Fig. 4. The input data of the fuzzy statistical normalizer are the fuzzy active sonar data, which are the output data of the linear law detector, and after the fuzzy statistical normalization, they are transformed into the crisp Rayleigh reverberation data as the output data. The input data of the FSN-CFAR detector are the normalized data that are the output of the fuzzy statistical normalizer and the original fuzzy sonar data. The normalized data are mainly used to estimate the background level, while the original fuzzy data, including clutter data and signal data, are mainly used to detect the target signals.

The structure of the FSN-CFAR detector is depicted in Fig. 5. Here, x_{CUT} is the CUT, $x_1 \ldots x_{N/2}$ are the leading reference cells, $x_{N/2+1} \ldots x_N$ are the lagging reference cells, and the shadow cells are guard cells that prevent target energy from corrupting the reference window. $aver1$, $aver2$, and $aver$ are the average values of the leading reference window, lagging reference window, and total reference data, respectively. Th_{edge} is the threshold that is employed to determine whether the leading reference window and the lagging reference window are homogeneous. If the average value of the leading reference window is greater than Th_{edge} times of the average value of the lagging reference window or is smaller than $\frac{1}{Th_{edge}}$ times of the average value of the lagging reference window, then the FSN-CFAR detector considers that the leading reference window and the lagging reference window are not homogeneous and takes the greater average value as the estimated background level. T_s and T_g are the proportion thresholds that decide

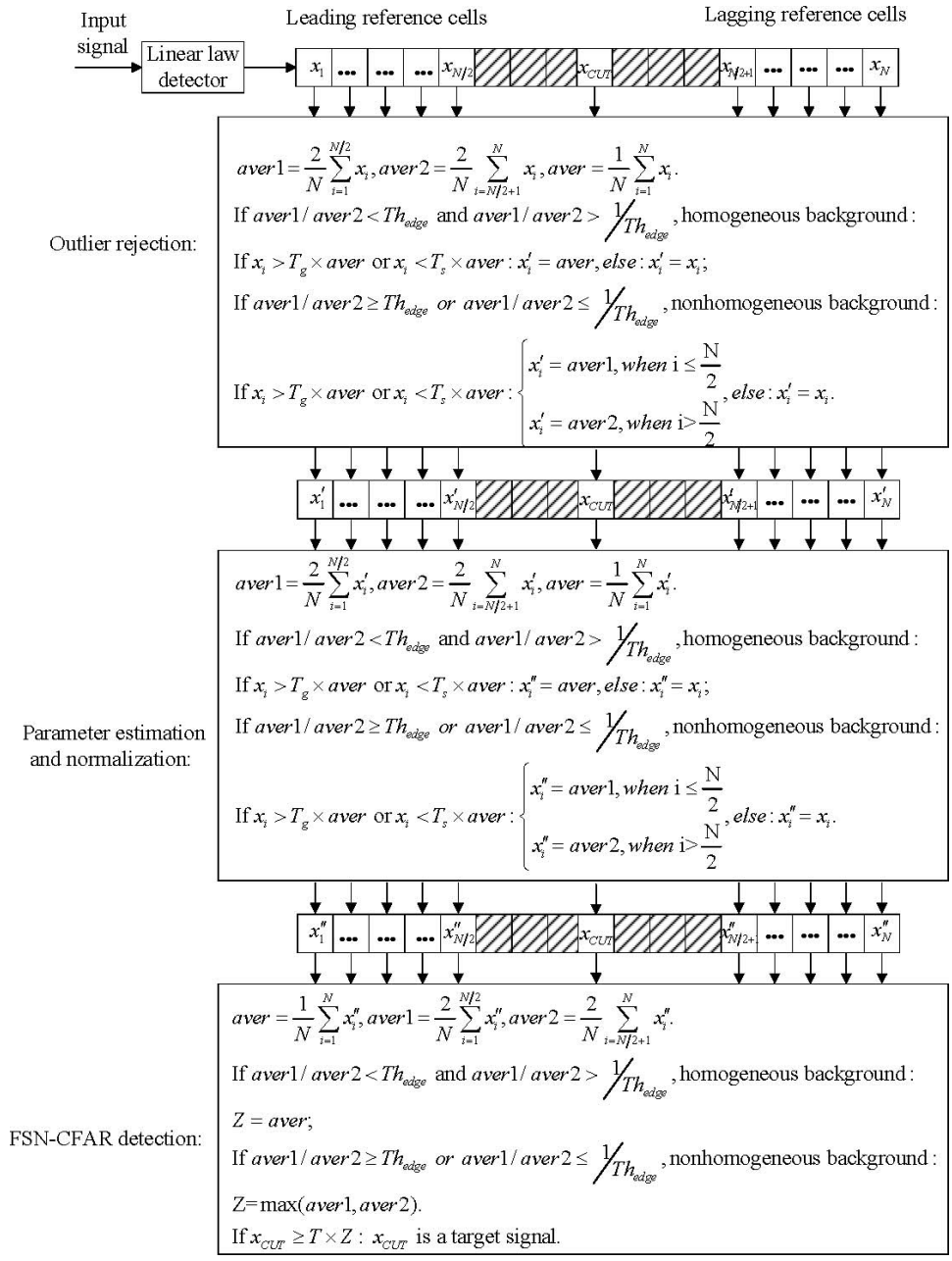

Fig. 5. FSN-CFAR detector.

whether x_i is an outlier, and they are deduced by (16). $x'_1 \ldots x'_{N/2}$ and $x'_{N/2+1} \ldots x'_N$ are the first normalized data that are used to estimate the parameter σ of the reference data. With $x'_1 \ldots x'_{N/2}$ and $x'_{N/2+1} \ldots x'_N$, the parameter σ of the membership function of the fuzzy Rayleigh set is gained. Based on the fuzzy Rayleigh set and the method of defuzzification, the second normalized data $x''_1 \ldots x''_{N/2}$ and $x''_{N/2+1} \ldots x''_N$ are obtained, and they are used to estimate the background level Z and determine the threshold parameter T for the FSN-CFAR detection. T is the threshold parameter to control the desired pf and is related to the distribution of the reference data, for example, different values of shape parameter v of K distribution will lead to different values of T. For a high-resolution radar or sonar system, the radar or sonar data are usually non-Rayleigh distributed and nonhomogeneous. It is impossible to completely normalize the non-Rayleigh and nonhomogeneous data to a Rayleigh distribution with the fuzzy statistical normalization. In fact, the normalization only makes the K-distribution shape parameter become larger, but it realizes the important purpose of outlier rejection. In this paper, we presume that the non-Rayleigh background data are K distributed; how to obtain the K-distribution shape parameter v is shown in [8–14]. In the proposed FSN-CFAR detector, the K-distribution shape parameter v should be estimated with the second normalized data $x''_1 \ldots x''_{N/2}$ and $x''_{N/2+1} \ldots x''_N$ when the second normalized

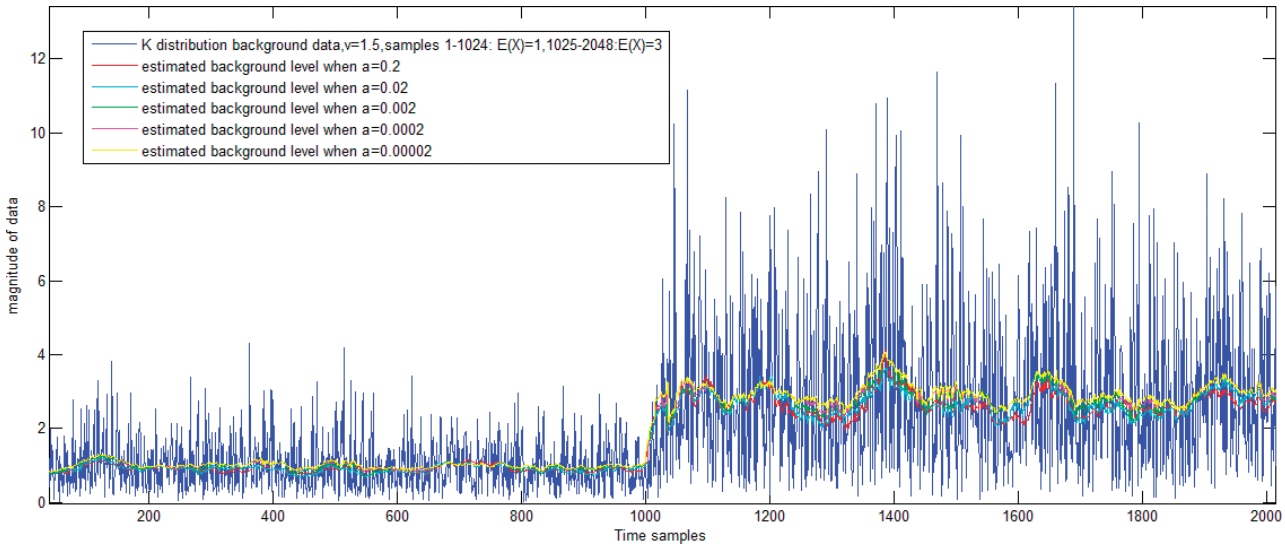

Fig. 6. Estimated background level of FSN-CFAR with different α values.

data are homogeneous. If the data are nonhomogeneous, that is, if $aver1 = \frac{2}{N}\sum_{i=1}^{N/2} x_i'', aver2 = \frac{2}{N}\sum_{i=N/2+1}^{N} x_i''$ and ($aver1/aver2 \geq Th_{edge}$ or $aver1/aver2 \leq 1/Th_{edge}$), the shape parameter v should be estimated with $x_1'' \ldots x_{N/2}''$, if $aver1 \geq aver2$, or with $x_{N/2+1}'' \ldots x_N''$, if $aver1 < aver2$. The threshold parameter T is acquired based on the estimated shape parameter v and the desired pf.

The proportion threshold T_s is deduced as follows:

From Section II.D, we know that the fuzzy data are transformed into normalized Rayleigh data using alpha-cut ($\alpha-$cut) method. We let $\alpha = 0.2$ and $\mu_A(x_{\min}, \sigma) = 0.2$. Based on (12), if $x < x_{\min}$, then $\mu_A(x, \sigma) < \mu_A(x_{\min}, \sigma)$, $P_R(x) < P_R(x_{\min}) = 0.1$, and x will be an outlier. Otherwise x will be a membership of the Rayleigh reverberation set.

Let $P_R(x_{\min}) = 0.1$, the relationship between $x_{\min}$ and the parameter σ is

$$\exp\left(-\frac{{x_{\min}}^2}{2\sigma^2}\right) = 0.9. \tag{17}$$

Based on (2), (3), and (17), the proportion of $x_{\min}$ to the $E(X)$ of the Rayleigh distribution variables can be calculated, here X is the reference data set. That is $T_s = \frac{x_{\min}}{E(X)} \approx 0.3663$, and the reference data whose value is smaller than $0.3663 \times E(X)$ will be rejected and replaced by $E(X)$.

That is, based on (2), (3), (12), and (17):

$$\mu_A(x_{\min}, \sigma) = 0.2, \rightarrow P_R(x_{\min}) = 0.1,$$
$$\rightarrow \exp\left(-\frac{{x_{\min}}^2}{2\sigma^2}\right) = 0.9, \rightarrow$$
$$\frac{{x_{\min}}^2}{\sigma^2} \approx 0.2107, \rightarrow \frac{{x_{\min}}^2}{(E(X))^2} \approx 0.1341,$$
$$\rightarrow T_s = \frac{x_{\min}}{E(X)} \approx 0.3663.$$

Similarly, the proportion threshold T_g is deduced as follows:

We let $\alpha = 0.2$ and $\mu_A(x_{\max}, \sigma) = 0.2$. Based on (12), if $x > x_{\max}$, then $\mu_A(x, \sigma) < \mu_A(x_{\max}, \sigma)$, $P_R(x) > P_R(x_{\max}) = 0.9$, and x will be an outlier. Otherwise, x will be a membership of the Rayleigh distribution set.

Let $P(x_{\max}) = 0.9$, the relationship between $x_{\max}$ and parameter σ is

$$\exp\left(-\frac{{x_{\max}}^2}{2\sigma^2}\right) = 0.1. \tag{18}$$

Based on (2), (3), and (18), the proportion of $x_{\max}$ to the $E(X)$ of the Rayleigh distribution variables can be calculated. That is, $T_g = \frac{x_{\max}}{E(X)} \approx 1.7122$, and the reference data whose value is greater than $1.7122 \times E(X)$ will be rejected and replaced by $E(X)$.

That is, based on (2), (3), (12), and (18):

$$\mu_A(x_{\max}, \sigma) = 0.2, \rightarrow P_R(x_{\max}) = 0.9,$$
$$\rightarrow \exp\left(-\frac{{x_{\max}}^2}{2\sigma^2}\right) = 0.1, \rightarrow$$
$$\frac{{x_{\max}}^2}{\sigma^2} \approx 4.605, \rightarrow \frac{{x_{\max}}^2}{(E(X))^2} \approx 2.9317,$$
$$\rightarrow T_g = \frac{x_{\max}}{E(X)} \approx 1.7122.$$

III. RESULTS AND DISCUSSIONS

From Section II, we know that the defuzzification transforms the fuzzy data into the crisp Rayleigh reverberation data using the $\alpha-$cut method. How do we assign the α value and will the changes of the α value influence the performance of FSN-CFAR detection? Fig. 6 shows the estimated background level of the FSN-CFAR with $\alpha = 0.2,\ 0.02,\ 0.002,\ 0.0002,\ 0.00002$, respectively. The parameter v of the simulated K-distribution data is 1.5. The number of the reference cells of the FSN-CFAR is 2×32, that is, $N = 64$. From

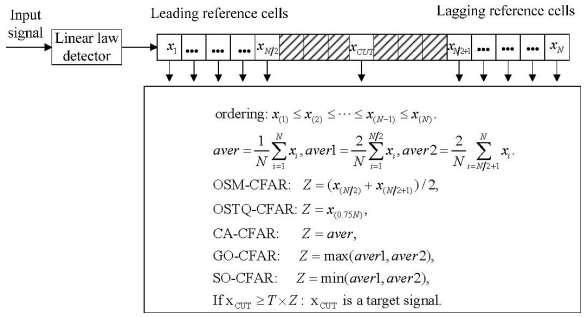

Fig. 7. Conventional detectors of OS-CFAR, CA-CFAR, GO-CFAR and SO-CFAR.

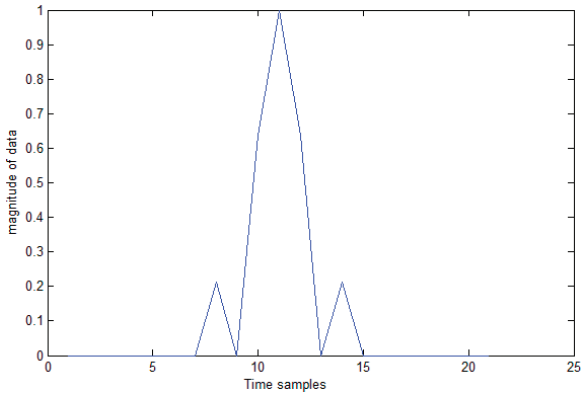

Fig. 8. Simulated target signal.

Fig. 6, we can see that the changes of the α value have little influence on the background level estimation of the FSN-CFAR detector in that the outliers are replaced by the average of the normalized reference cells.

To illustrate the detection performance of the FSN-CFAR detector in a non-Rayleigh background, we compared its probability of detection (pd) to conventional detectors using the Monte-Carlo simulation method. All of the different signal-to-noise ratio (SNR) target signals and the K-distribution background data with different shape parameters were obtained through simulation. The conventional detectors are CA-CFAR, GO-CFAR, SO-CFAR, and OS-CFAR, which are displayed in Fig. 7. The α value of the FSN-CFAR detector is 0.2, that is, $T_s = 0.3663$ and $T_b = 1.7122$. Here, we call OS-CFAR OSM-CFAR when the background level Z is taken to be equal to the median of the reference cells values, we and call OS-CFAR OSTQ-CFAR when $Z = x_{(i)}$ and the rank-ordered index i is taken to be equal to three-quarters of N. All the conventional detectors and the proposed FSN-CFAR detector have the same reference window size and guard window size. In view of the high resolution of the modern sonar or radar data, here the lengths of the reference window, the guard window, and the simulated signal are 2×64, 2×32, and 9, respectively. The simulated target signal is attained by a sinc function and is shown in Fig. 8.

For the conventional detectors, the non-Rayleigh distribution parameters of the background data are not changed before the detection threshold is achieved. Thus, if we assume that the non-Rayleigh background data are K distributed and the shape parameters of the K distribution are the same, the detection performances of the conventional detectors can be compared under the same conditions by simulation method. For the proposed FSN-CFAR detector, the statistical normalization changes the K-distribution shape parameter of the background data, and the normalized background data may not follow K distribution completely. Furthermore, even the normalized data follow K distribution, and it is difficult to ensure every group normalized data have the same shape parameter and to estimate the K-distribution shape parameter precisely in the Monte-Carlo simulation trials; all these will influence the simulation results in the FSN-CFAR detection. For the previously mentioned reasons, there are two assumptions in the Monte-Carlo simulation trials in this paper: the first assumption is that the non-Rayleigh background data are K distributed and the shape parameter v of the K distribution is known; and the second is that after the fuzzy statistical normalization, the K-distribution shape parameter of the normalized background data is not changed. Based on the second assumption, the FSN-CFAR need not estimate the K-distribution shape parameter with the normalized background data, for the shape parameter of the normalized background data is not changed.

Based on the two assumptions, the statistical simulated results of pd and pf of the conventional detectors and the proposed FSN-CFAR detector are obtained under the same conditions.

Fig. 9 depicts the false-alarm rate of the FSN-CFAR, CA-CFAR, SO-CFAR, GO-CFAR, OSM-CFAR, and OSTQ-CFAR detectors versus threshold parameter T, with $N = 2 \times 64$, for the K-distribution shape parameter: Fig. 9a: $v = 5.0$; Fig. 9b: $v = 3.5$; Fig. 9c: $v = 1.5$; and Fig. 9d: $v = 0.5$. All the results of Fig. 9 were acquired using Monte-Carlo simulation with 200 000 independent trials. It can be observed that the larger K-distribution shape parameter v is, the smaller the threshold parameter T required to reach a given pf is. Based on Fig. 9, the threshold parameter T for a given pf for the FSN-CFAR, CA-CFAR, SO-CFAR, GO-CFAR, OSM-CFAR, and OSTQ-CFAR detectors in the K-distribution background with shape parameter $v = 5.0, 3.5, 1.5, 0.5$ can be attained.

To evaluate the detection performance of the FSN-CFAR detector under K-distribution background, several computer simulations have been conducted. Multiple target situations and the case in which a clutter edge is present in the reference widow are considered. All the detection simulation results are obtained by the Monte Carlo method, with 10^5 independent trials with the design $pf = 10^{-3}$ and the window size $N = 2 \times 64$.

In Figs. 10–12, the performances of the FSN-CFAR detector are compared with the CA-CFAR, GO-CFAR, SO-CFAR, and OS-CFAR detectors by using the plotted

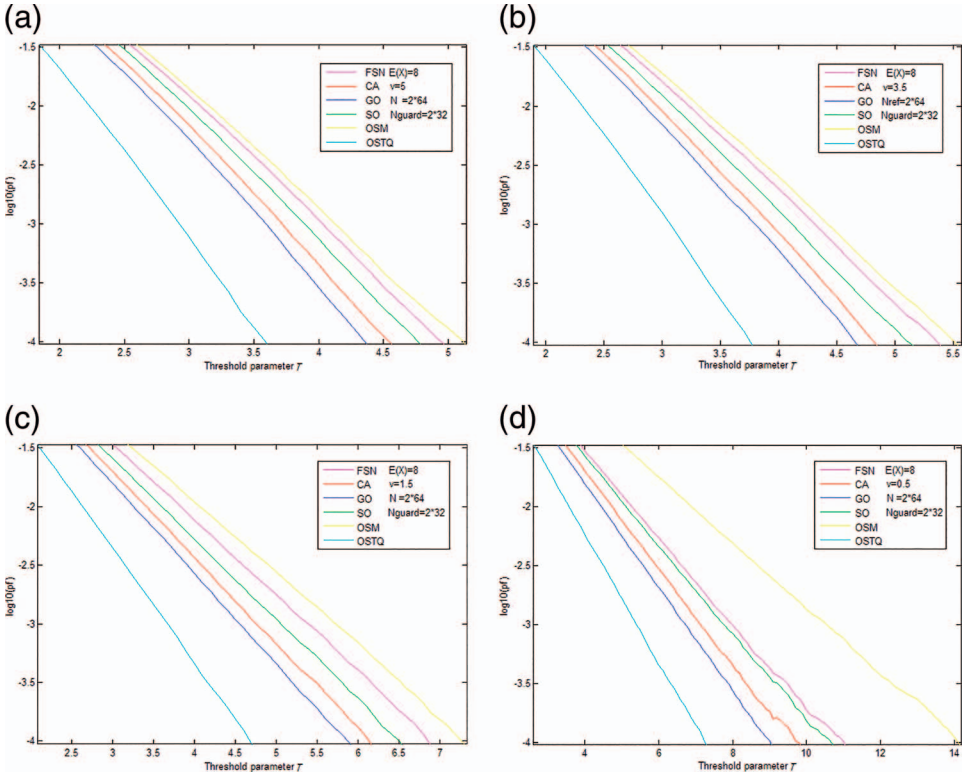

Fig. 9. Pf of different CFAR detectors versus threshold parameter T, for shape parameter: (a) $v = 5.0$; (b) $v = 3.5$; (c) $v = 1.5$; (d) $v = 0.5$.

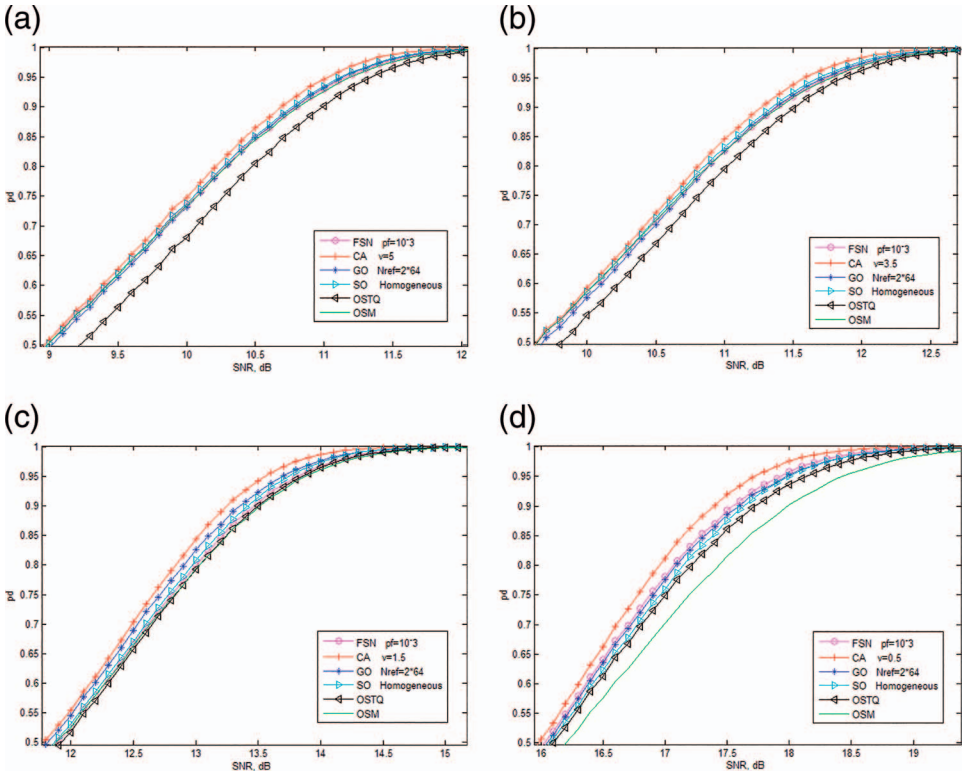

Fig. 10. Pd against SNR of FSN-CFAR, CA-CFAR,GO-CFAR,SO-CFAR and OS-CFAR detectors in homogeneous K distribution background, for shape parameter: (a) $v = 5.0$; (b) $v = 3.5$; (c) $v = 1.5$; (d) $v = 0.5$, $N = 2 \times 64$, design $pf = 10^{-3}$.

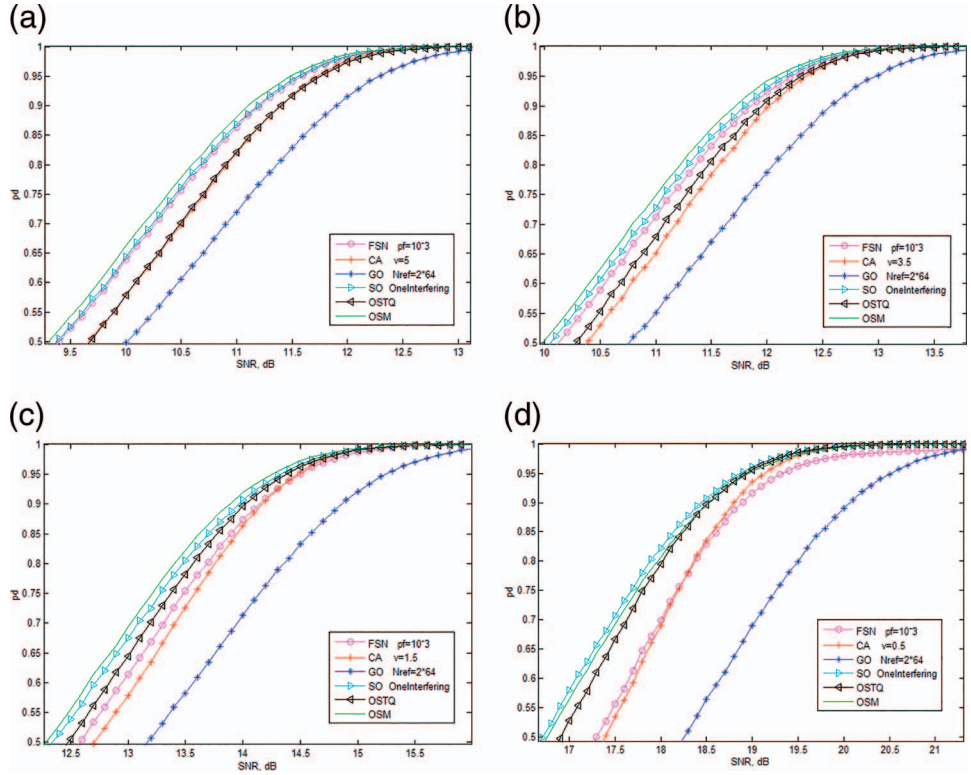

Fig. 11. Pd against SNR of FSN-CFAR, CA-CFAR,GO-CFAR,SO-CFAR and OS-CFAR detectors in K-distribution background with one interfering target in leading reference window with $INR = SNR$, for shape parameter: (a) $v = 5.0$; (b) $v = 3.5$; (c) $v = 1.5$; (d) $v = 0.5$; $N = 2 \times 64$, design $pf = 10^{-3}$, $INR = SNR$.

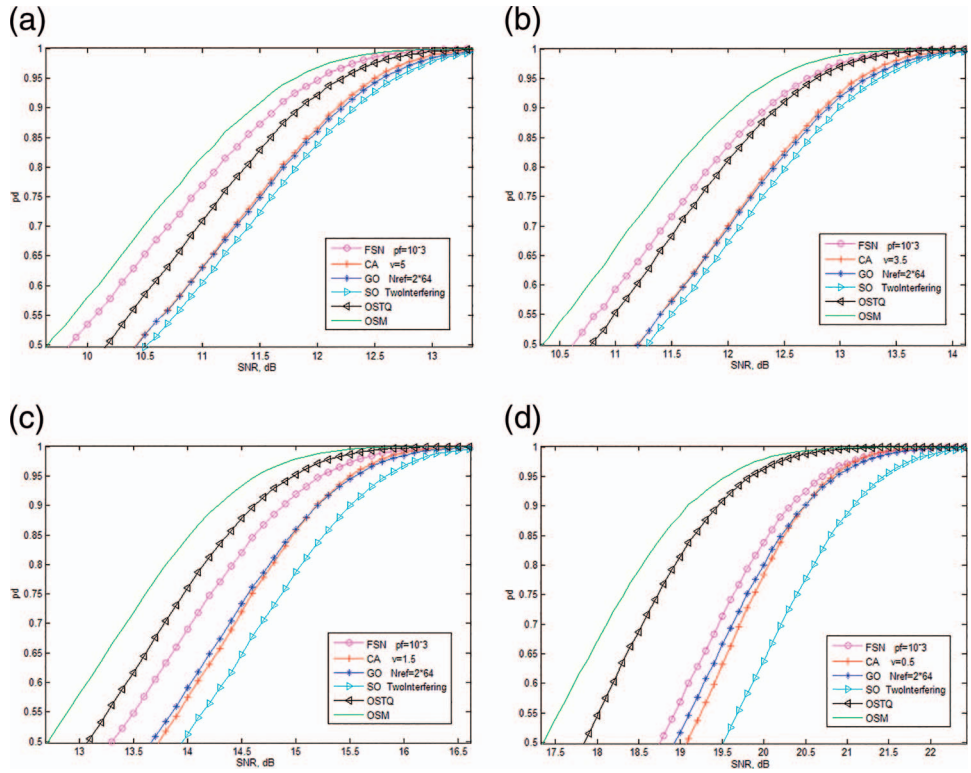

Fig. 12. Pd against SNR of FSN-CFAR, CA-CFAR,GO-CFAR,SO-CFAR and OS-CFAR detectors in K-distribution background with one interfering target in leading reference window and one in lagging reference window with $INR = SNR$, for shape parameter: (a) $v = 5.0$; (b) $v = 3.5$; (c) $v = 1.5$; (d) $v = 0.5$, $N = 2 \times 64$, design $pf = 10^{-3}$.

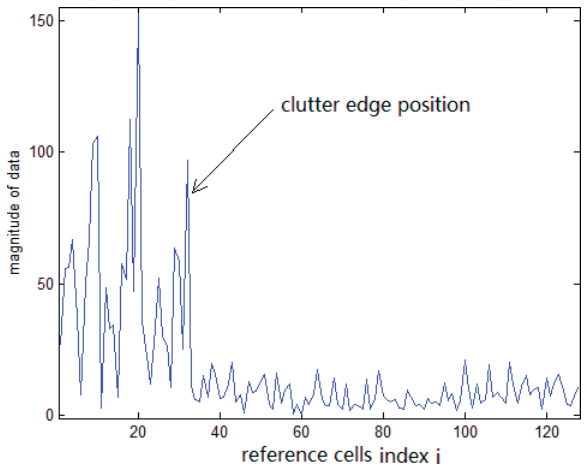

Fig. 13. Power transition of simulated reference window.

pd as a function of SNR curves. Fig. 10 depicts the pd against the SNR of FSN-CFAR, CA-CFAR, GO-CFAR, SO-CFAR, and OS-CFAR detectors in a homogeneous K-distribution background, for shape parameter: Fig. 10a: $v = 5.0$; Fig. 10b: $v = 3.5$; Fig 10c: $v = 1.5$; and Fig. 10d: $v = 0.5$. Fig. 11 depicts the pd against the SNR in K-distribution background with one interfering target in the leading reference window with $INR = SNR$, for shape parameter: Fig. 11a: $v = 5.0$; Fig. 11b: $v = 3.5$; Fig. 11c: $v = 1.5$; and Fig. 11d: $v = 0.5$, with the interfering target-to-noise ratio (INR). Fig. 12. depicts Pd against the SNR in K-distribution background with one interfering target in the leading reference window and one interfering target in the lagging reference window with $INR = SNR$, for shape parameter Fig. 12a: $v = 5.0$; Fig. 12b: $v = 3.5$; Fig. 12c: $v = 1.5$; and Fig. 12d: $v = 0.5$.

Fig. 10 shows that the CA-CFAR detector has the best performance when the background is homogenous, while the detection performances of the OS-CFAR detectors are poor. From Figs. 11 and 12, we can see that the performances of the GO-CFAR, SO-CFAR, and CA-CFAR detectors are poor when both the leading reference window and the lagging reference window have one or more interfering targets. The detection performance of the FSN-CFAR is robust or moderate compared with the other CFAR detectors. However, all the results are obtained under the assumption that after the fuzzy statistical normalization, and the K-distribution shape parameter of the normalized background data is not changed. In fact, after the fuzzy statistical normalization, the extended upper tail data are attenuated, and the shape parameter should become larger. From Figs. 10–12, we can see that for all the detectors, the larger K-distribution shape parameter of the background data, the better detection performance of the CFAR detector is. Thus, we can believe that if we estimate the K-distribution shape parameter with the normalized background data in the proposed FSN-CFAR detector, the shape parameter should become larger, and the detection performance may be better than the simulation results in this paper, especially in the condition of the K-distribution shape parameter being smaller.

The effects of clutter edges on the false-alarm performances of the FSN-CFAR, CA-CFAR, SO-CFAR, GO-CFAR, OSM-CFAR, and OSTQ-CFAR detectors are analyzed using the Monte Carlo method with 10^6

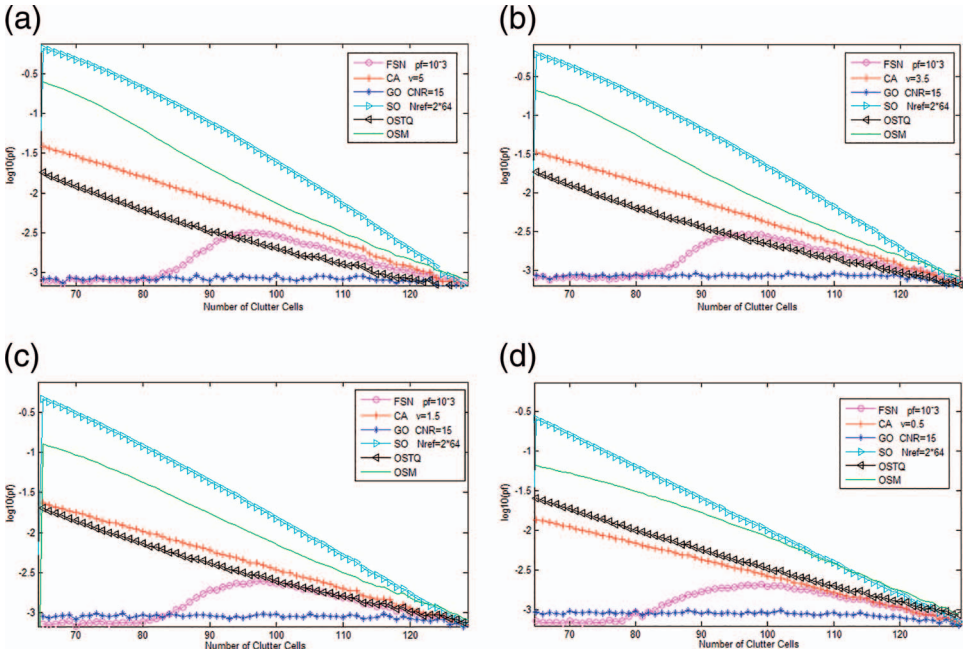

Fig. 14. Pf comparison of FSN-CFAR, CA-CFAR, GO-CFAR, SO-CFAR and OS-CFAR detectors in clutter edge (15-dB CNR) environment, for shape parameter: (a) $v = 5.0$; (b) $v = 3.5$; (c) $v = 1.5$; (d) $v = 0.5$, $N = 2 \times 64$, design $pf = 10^{-3}$.

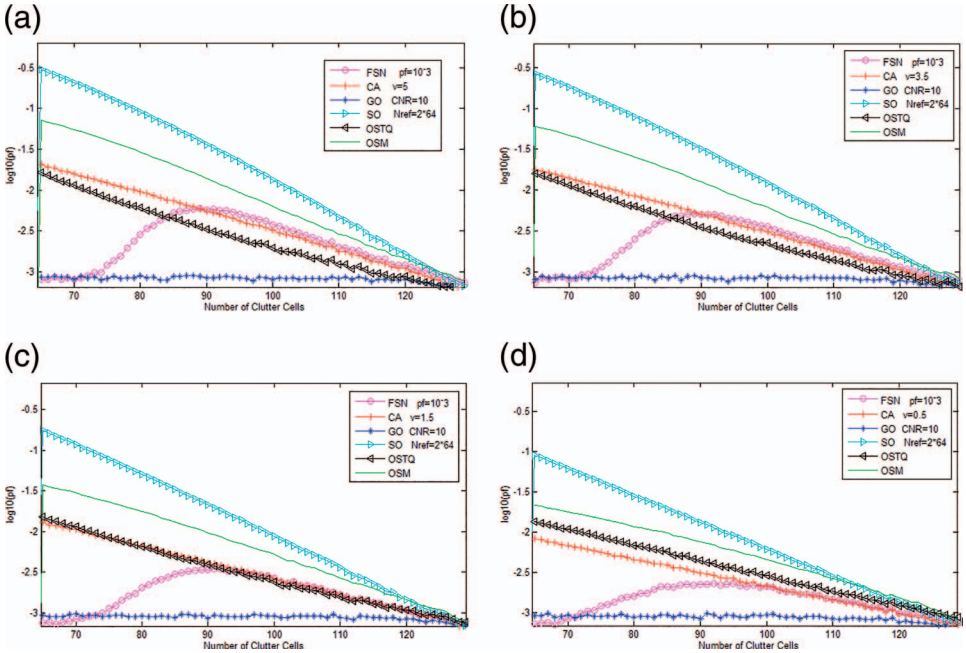

Fig. 15. Pf comparison of FSN-CFAR, CA-CFAR, GO-CFAR, SO-CFAR and OS-CFAR detectors in clutter edge (10 dB CNR) environment, for shape parameter: (a) $v = 5.0$; (b) $v = 3.5$; (c) $v = 1.5$; (d) $v = 0.5$; $N = 2 \times 64$, design $pf = 10^{-3}$.

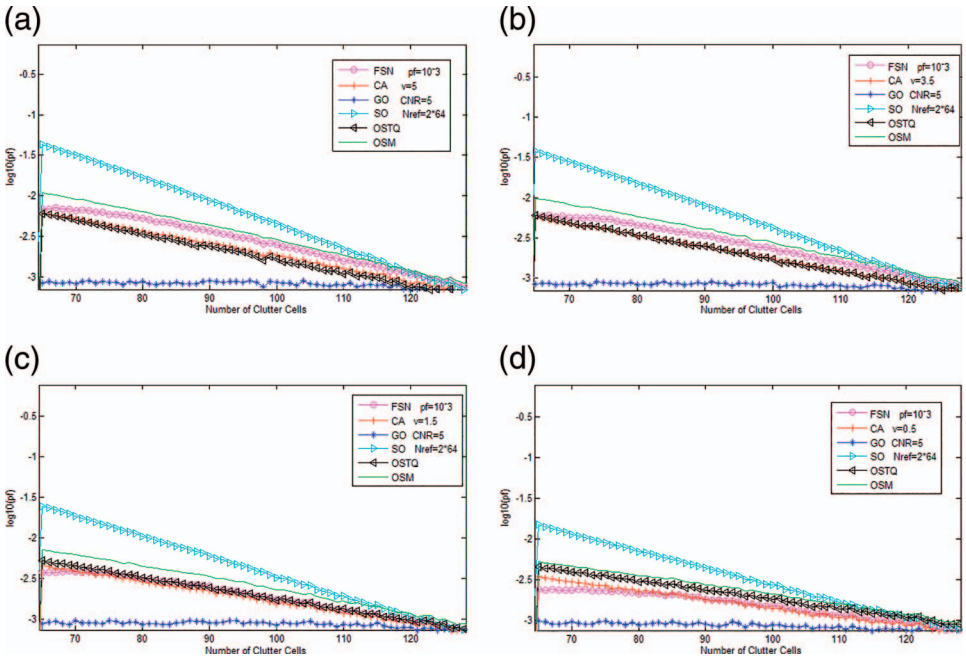

Fig. 16. Pf comparison of FSN-CFAR, CA-CFAR, GO-CFAR, SO-CFAR and OS-CFAR detectors in clutter edge (5-dB CNR) environment, for shape parameter: (a) $v = 5.0$; (b) $v = 3.5$; (c) $v = 1.5$; (d) $v = 0.5$; $N = 2 \times 64$, design $pf = 10^{-3}$.

independent trials, with the design $pf = 10^{-3}$, the reference window size $N = 2 \times 64$, and the threshold $Th_{edge} = 1.9$.

Fig. 13 shows the power transition of the simulated reference window: the left reference cells of the clutter edge position are clutter, and the right reference cells are noise.

The pf in a clutter edge environment for the CFAR detectors is shown in Figs. 14–16, where the clutter-to-noise ratio (CNR) is, respectively, 15 dB, 10 dB, and 5 dB, and Figs. 14–16 illustrate the curves of pf versus clutter edge position. If the position of the clutter edge in the reference window is smaller than 64, then the real pf will be lower than the design pf, so Figs. 14–16 only show the curves of pf when the clutter edge position is greater than 64.

Figs. 14–16 show that the pf of SO-CFAR, OSM-CFAR, CA-CFAR, and OSTQ-CFAR deviates from

the design pf abruptly when the clutter edge is located around the CUT. GO-CFAR always outperforms the other CFAR detectors, and FSN-CFAR outperforms the GO-CFAR when the clutter edge is located around the CUT and $20\log_{10}(Th_{edge}) < CNR$.

IV. CONCLUSION AND FUTURE WORK

In this paper, a robust FSN-CFAR detector, based on fuzzy statistical normalization is proposed. We have compared the performance of the proposed FSN-CFAR detector with the conventional CFAR detectors, such as CA-CFAR, GO-CFAR, SO-CFAR, and OS-CFAR in nonhomogeneous environment and non-Rayleigh background. Simulation results show that the performances of SO-CFAR and OSM-CFAR detectors are poor in the case of a clutter edge. GO-CFAR offers good performance in a clutter edge environment, but its detection performance is poor in multiple target situations. The performance of CA-CFAR is the best in homogeneous background, but FSN-CFAR outperforms CA-CFAR in nonhomogeneous background and offers low CFAR loss in homogeneous background. Compared with OSTQ-CFAR, the superiority of FSN-CFAR is perceptible: OSTQ-CFAR offers higher CFAR loss in homogeneous background and higher pf in clutter edge environments and is very time consuming when the number of reference cells is large. The proposed FSN-CFAR may be a robust CFAR detector for non-Rayleigh radar or sonar data both in nonhomogeneous and homogeneous environments.

The detectors are compared on the basis that the clutter is K distributed with a known shape parameter in this paper. Although in reality, the true clutter distribution is unknown, and the shape parameter of the K distribution must be estimated from the data. It is difficult to get accurate estimates from small samples as required for a practical CFAR detector. This could have an impact on the performance of the proposed detector. We defer detailed consideration and simulation of this important issue in future work.

REFERENCES

[1] Finn, H. M., and Johnson, R. S.
Adaptive detection mode with threshold control as a function of spatially sampled clutter level estimate.
RCA Review, **29**, 3 (Sep. 1968), 414–464.

[2] Trunk, G. V.
Range resolution of targets using automatic detectors.
IEEE Transactions on Aerospace and Electronic Systems, **14**, 5 (Sep. 1978), 750–755.

[3] Hansen, G. V., and Sawyers, J. H.
Detectability loss due to greatest-of selection in a cell averaging CFAR.
IEEE Transactions on Aerospace and Electronic Systems, **16**, 1 (1980), 115–118.

[4] Rohling, H.
Radar CFAR thresholding in clutter and multiple target situations.
IEEE Transactions on Aerospace and Electronic Systems, **19**, 4 (July 1983), 608–621.

[5] Gandhi, P. P., and Kassam, S. A.
Analysis of CFAR processors in nonhomogeneous background.
IEEE Transactions on Aerospace and Electronic Systems, **24**, 4 (1988), 427–445.

[6] Weiss, M.
Analysis of some modified cell-averaging CFAR processors in multiple-target situations.
IEEE Transactions on Aerospace and Electronic Systems, **18**, 1 (1982), 102–114.

[7] Abraham, D. A.
Choosing a non-Rayleigh reverberation model.
In *Proceedings of the OCEANS Conference*, Seattle, WA, 1999, 284–288.

[8] Raghavan, R. S.
A method for estimating parameters of K-distributed clutter.
IEEE Transactions on Aerospace and Electronic Systems, **27**, 2 (1991), 238–246.

[9] Blacknell, D. and Tough, R. J. A.
Parameter estimation for the K-distribution based on [z log(z)].
IEE Proceedings Radar, Sonar and Navigation, **148**, 6 (2001), 309–312.

[10] Iskander, D. R., and Zoubir, A. M.
Estimation of the parameters of the K-distribution using higher order and fractional moments.
IEEE Transactions on Aerospace Electronic Systems, **35**, 4 (1999), 1453–1457.

[11] Roberts, W. J. J., and Furui, S.
Maximum likelihood estimation of K-distribution parameters via the expectation-maximization algorithm.
IEEE Transactions on Signal Processing **48**, 12 (2000), 3303–3306.

[12] Mezache, A., and Soltani, F.
A new approach for estimating the parameters of the K-distribution using fuzzy-neural networks.
IEEE Transactions on Signal Processing, **56**, 11 (2008), 5724–5728.

[13] Fialkowski, J. M., and Gauss, R. C.
Methods for identifying and controlling sonar clutter.
IEEE Journal of Oceanic Engineering, **35**, 2 (2010), 330–354.

[14] Abraham, D. A., and Lyons, A. P.
Reliable methods for estimating the distribution shape parameter.
IEEE Journal of Oceanic Engineering, **35**, 2 (2010), 288–302.

[15] Meng, X. W.
Performance analysis of OS-CFAR with binary integration for Weibull background.
IEEE Transactions on Aerospace and Electronic Systems, **49**, 2 (2013), 1357–1366.

[16] Anastassopoulos, V., and Lampropoulos, G.
Optimal CFAR detection in Weibull clutter.
IEEE Transactions on Aerospace and Electronic Systems, **48**, 2 (2012), 1747–1758.

[17] Pourmottaghi, A., Taban, M. R., and Gazor, S.
A CFAR detector in a nonhomogenous Weibull clutter.
IEEE Transactions on Aerospace and Electronic Systems, **31**, 1 (1995), 52–64.

[18] Rifkin, R.
Analysis of CFAR performance in Weibull clutter.
IEEE Transactions on Aerospace and Electronic Systems, **30**, 2 (1994), 315–328.

[19] Guida, M., Longo, M., and Lops, M.
Biparametric linear estimation for CFAR against Weibull clutter.
IEEE Transactions on Aerospace and Electronic Systems, **28**, 1 (1992), 138–151.

[20] Goldstein, G. B.
False-alarm regulation in log-normal and Weibull clutter.
IEEE Transactions on Aerospace and Electronic Systems, **9**, 1 (1973), 84–92.

[21] Gu, M., and Abraham, D. A.
Using McDaniel's model to represent non-Rayleigh reverberation.
IEEE Journal of Oceanic Engineering, **26**, 3 (2001), 348–357.

[22] Abraham, D. A., Gelb, J. M., and Oldag, A. W.
Background and clutter mixture distributions for active sonar statistics.
IEEE Journal of Oceanic Engineering, **36**, 2 (2011), 231–247.

[23] La Cour, B. R.
Statistical characterization of active sonar reverberation using extreme value theory.
IEEE Journal of Oceanic Engineering, **29**, 2 (2004), 310–316.

[24] Barnard, T. J., and Khan, F.
Statistical normalization of spherically invariant non-Gaussian clutter.
IEEE Journal of Oceanic Engineering, **29**, 2 (2004), 303–309.

[25] Leung, S. W., and Minett, J. W.
The use of fuzzy spaces in signal detection.
Fuzzy Sets and Systems, **114**, 2 (2000), 175–184.

[26] Leung, S. W., and Minett, J. W.
A fuzzy approach to signal integration.
IEEE Transactions on Aerospace and Electronic Systems, **38**, 1 (2002), 346–351.

[27] Hammoudi, Z., and Soltani, F.
Distributed CA-CFAR and OS-CFAR detection using fuzzy spaces and fuzzy fusion rules.
IEE Proceedings Radar, Sonar and Navigation, **151**, 3 (2004), 135–142.

[28] Hao, C., Cai, L., and Chen, M.
Distributed ODV-CFAR detection based on fuzzy logic.
In *Proceedings of the International Workshop on Intelligent Systems and Applications*, Wuhan, China, May 2009.

[29] Gamal, M., Attala M., and Hafez, A. S.
A new fuzzy CFAR processor for radar MTD systems.
In *Proceedings of the IEEE Aerospace Conference*, Big Sky, MT, Mar. 2012.

[30] Newhall, B. K.
A physical model for the distribution of sonar clutter from a rough interface.
In *Proceedings of the IEEE OCEANS Conference*, Boston, MA, 2006.

[31] Minett, J. W., Leung, S. W., Siu Y. M., Ng, K. T., and Chau, W. N.
Estimating the length of a radar shadow in shadow-feature-enhanced detection using a fuzzy system.
In *Proceedings of 10th IEEE International Conference on Fuzzy Systems*, Melbourne, Australia, 2001, 115–118.

Yanwei Xu received a B.Sc. degree in electrical automation from Qingdao University of Science and Technology, Qingdao, China, in 2001. He received a M.Sc. degree in control theory and control engineering from the University of Science and Technology Beijing, China, in 2004. He received a Ph.D. degree in signal and information processing from Institute of Acoustics, Chinese Academy of Sciences (IACAS), Beijing, China, in 2012.

In 2004, he joined IACAS and was a Postdoctoral Research Associate with the IACAS, Beijing, China, from 2012 to 2014. His main research interest is signal processing based on uncertainty theories and cognitive techniques, especially with active sonar or radar systems in a complex and uncertain environment.

Chaohuan Hou (SM'96—F'01) received a B.Sc. degree in physics from Peking University, Beijing, China, in 1958.

Since 1958, he has worked on underwater acoustics and signal processing with the IACAS, Beijing, where he became a professor in 1985. He was the Deputy Director of IACAS from 1993 to 1997.

He has published more than 200 journal and conference papers. His current research interests are in underwater acoustics, digital signal processing, arrays signal processing, very-large-scale integration signal processing, and application-specific integrated circuit chip design.

Prof. Hou was elected as an academician of the Chinese Academy of Sciences in 1995. He was the president of the Acoustical Society of China from 2002 to 2006 and then became the honorary president. From 2007 to 2010, he was a board member of the International Commission for Acoustics.

Shefeng Yan (M'05—SM'10) received B.Sc., M.Sc., and Ph.D. degrees in electrical engineering from Northwestern Polytechnical University, Xi'an, China, in 1999, 2001, and 2005, respectively.

He was a postdoctoral research associate with IACAS, Beijing, China, from 2005 to 2007, and with the Department of Electronics and Telecommunications, Norwegian University of Science and Technology, Trondheim, Norway, from 2007 to 2009, respectively. In 2009, he joined IACAS as a professor and was then appointed as the director of the Intelligent Sensing and Signal Processing Lab at IACAS. He is the author of the book *Sensor Array Beampattern Optimization: Theory with Applications* (Science Press, 2009). His current research interests include underwater acoustics, statistical and array signal processing, and their applications.

Professor Yan is an outstanding young scholar of "Hundred Talents Program" with the Chinese Academy of Sciences. He is a recipient of the Chinese 2008 National Excellent Doctoral Dissertation Award, as well as a recipient of the 2010 International Commission on Acoustics–Acoustical Society of America Young Scientist Grant for excellent contributions to acoustics. He is also a corecipient of the Best Paper Awards at Sensor Technologies and Applications 2008 and Workshop on Applications of Signal Processing to Audio and Acoustics 2009.

Jun Li received his B.Eng. and M.Eng. degreees in electrical engineering and underwater acoustic engineering, respectively, from Harbin Engineering University in 1989 and 1997. He received his Ph.D. degree in information and signal processing from the Graduate University of Chinese Academy of Sciences in 2004. He worked as a visiting fellow at Princeton University in 2011 for 1 y.

He is now a professor at IACAS. His research interests include sonar systems and underwater acoustic signal processing. He won the Chinese State Advanced Science and Technique Prize in 2013 and Outstanding Achievement Honor in Science from the Chinese Academy of Sciences in 2014.

Chengpeng Hao (M'08) received B.S. and the M.S. degrees in electronic engineering from Beijing Broadcasting Institute, Beijing, China, in 1998 and 2001, respectively. He received the Ph.D. degree in signal and information processing from IACAS, Beijing, China, in 2004. He has held a visiting position with the Electrical and Computer Engineering Department, Queen's University, Kingston, Canada (July 2013–July 2014).

He is currently a professor in the State Key Laboratory of Acoustics, IACAS. His research interests are in the field of statistical signal processing, with more emphasis on adaptive sonar and radar signal processing. He won Chinese State Advanced Science and Technique Prize in 2013 and Outstanding Achievement Honor in Science from the Chinese Academy of Sciences in 2014.